Available online at www.sciencedirect.com
ScienceDirect
Trans. Nonferrous Met. Soc. China 34(2024) 1507−1519
Transactions of Nonferrous Metals Society of China
www.tnmsc.cn

Formation mechanism and mechanical behavior of gradient nanograin structure in directional solidified Ti_3Al alloy: Atomic-scale study

Peng-fei ZOU[1], Chang LI[1], Zhao-yang HOU[1], Jia-yi SUN[2],
Quan-hua GAO[1], Ke-fan LI[1], Zhen WANG[1], Ke-jun DONG[3]

1. School of Science, Chang'an University, Xi'an 710064, China;
2. Faculty of Natural, Mathematics & Engineering Sciences, King's College London, London, WC2R 2LS, United Kingdom;
3. School of Engineering, Design and Built Environment, Western Sydney University, Penrith, NSW 2751, Australia

Received 31 January 2023; accepted 16 August 2023

Abstract: The formation mechanism of Ti_3Al alloy during a directional solidification process was systemically investigated by means of molecular dynamics (MD) simulations, and its mechanical behavior was explored by comparing with its nanograined (NG), coarse-grained (CG) and gradient nanograined (GNG) counterparts. It is found that the solidified front forms equiaxed crystals first, then they transform into columnar crystals, and the GNG structure is formed finally. Noticeably, the grains will grow preferentially in the direction parallel to the solidification direction. Besides, it is also found that the directional solidified alloy with the GNG structure has higher tensile strength and better ductility than its NG and CG counterparts. The GNG structure not only suppresses strain localization and grain growth in its small grain regions, but also promotes more cross dislocations in the large grain regions, resulting in a better mechanical performance.

Key words: directional solidification; Ti_3Al alloy; molecular dynamics simulation; gradient nanograin structure

1 Introduction

Ti−Al alloys have the advantages of low density, high specific strength, and good high-temperature performance. Thus, they are widely applied in the aerospace and engine industry [1−3]. It is well known that the physical and mechanical properties of alloys are closely related to their microstructures, which is inextricably linked with the solidification process. Some new technologies for preparing materials are constantly being invented, and directional solidification is an excellent choice to improve the strength and ductility of Ti−Al alloy.

The grains of metallic materials prepared by directional solidification will eventually form a gradient structure. The grain size gradually increases from the low-temperature region to the high-temperature region. Alloys with gradient nanograins exhibit excellent mechanical properties during deformation [4−9]. YUE et al [4] studied the microstructure, fracture toughness and high-temperature tensile properties of Ti−46Al−5Nb−0.18C−0.3Si alloy prepared by the directional solidification method. It is found that the fracture toughness of the alloy increases with the increase of the orientation angle, and the fracture behavior changes from interlayer to cross-layer. The study also demonstrates that the well-aligned lamellar microstructure has excellent high-temperature tensile

Corresponding author: Zhao-yang HOU, E-mail: zhaoyanghou@163.com
DOI: 10.1016/S1003-6326(24)66487-3

property. LIU et al [5] studied the directional solidification process of Ti44Al6Nb1Cr alloy, and the results show that the microstructure of the alloy prepared by cold crucible directional solidification changes from equiaxed grains to columnar crystals growing along the axial direction, which leads to the remarkable improvement of the mechanical properties. For Ti−Al alloy prepared by directional solidification, the microstructural evolution exhibits similar behavior to that of Ti44Al6Nb1Cr alloy [6]. WANG et al [7] also prepared Ti−Al alloy with a gradient structure by cold crucible directional solidification, and studied the effects of grain size on the creep behavior and fracture toughness.

The excellent mechanical properties of gradient structure usually come from its unique plastic deformation mechanism. In gradient nanomaterials, there exist grains of various sizes, and their plastic deformation mechanisms are also different. Thus, it is essential to explore the multi-scale plastic deformation mechanism of the gradient nanograin (GNG) structure in directional solidified TiAl alloy. FANG et al [10] synthesized the GNG Cu structure with grain size increasing from 20 to 300 nm on the surface of coarse-grained Cu rods. The tensile experiment showed that the GNG layer can double the strength without sacrificing tensile ductility. Its plastic deformation is dominated by the mechanically driven grain boundary migration process of nanograins on the surface, which effectively suppresses strain localization. Indeed, the GNG structure is a typical non-uniform structure, and its strengthening mechanism is closely related to the evolution of geometrically necessary dislocations [11−13]. WU et al [12,13] utilized the stress relaxation approach to study the relationship between the movable dislocation density and the strain inside GNG interstitial-free steels. The movable dislocation density along the strain inside the grains falls first and then rises to equilibrium.

With the rapid development of high-performance computing, researchers have developed several computational methods to simulate the directional solidification process of metals, such as the phase field method [14−17], Monte Carlo [18] and molecular dynamics simulations [19−21]. Comparatively, the phase-field method can be used on larger and longer scales, while molecular dynamics (MD) simulation is more effective for studying atomistic-scale phenomena, especially for the solidification process of nano-structure metals. In recent years, some researchers have adopted MD to predict the evolution of nanostructures during the solidification process of different alloys [22−24], which promoted the development of directional solidification.

MAHATA and ASLE ZAEEM [19,20] studied the directional solidification process of Al−Cu and Mg−Al alloys by MD simulation. It is demonstrated that various defects, such as twins, stacking faults, and grain boundaries, occur in the alloy at the early stage of solidification, while no new defects are generated at the final stage of solidification. As for the solidification process of Mg−Al alloys, the alloys show heterogeneous characteristics due to the existence of several $Mg_{17}Al_{12}$ precipitates, which is different from the Al−Cu alloys. Some dislocations will slip around the grain boundaries when the deformation is along the growth direction of directional solidification. If the loading is perpendicular to the growth direction, more energy is needed to generate the defects compared to the parallel growth direction, which results in higher stretching stress for the parallel growth direction than that for the perpendicular growth direction. BAHRAMYAN et al [21] also simulated FeCrNi alloy by large-scale molecular dynamics simulation, and studied the relationships among the stacking faults (SF), dislocations (DS), grain boundaries (GB), internal stacking faults (ISF), and external stacking faults (ESF).

At present, the directional solidification process of Ti−Al alloys is mainly simulated by the phase-field method [25−29]. The formation mechanism of columnar grains during the directional solidification process of Ti_3Al alloy and its deformation mechanism under tensile are rarely studied at the atomistic scale. Thus, in this work, MD simulation is used to study the competitive growth between grains during the directional solidification of Ti_3Al alloy and the mechanical behavior of the directional solidification structures.

2 Computational method

The large-scale atomistic/molecular massively

parallel simulator (LAMMPS) [30] was used for conducting MD simulation. The motion equations are solved by the velocity-Verlet algorithm with a time step of 1 fs. For the interatomic potential, the typical EAM potential for Ti−Al alloy developed by ZOPE and MISHIN [31] was used, which can be expressed as

$$E_{\text{tot}} = \sum_{i=1}^{N-1} \sum_{j=i+1}^{N} \varphi_{ij}(r_{ij}) + \sum_{i=1}^{N} F_i(\rho_i) \quad (1)$$

where F_i is the embedding energy related to electron density ρ_i, and r_{ij} and φ_{ij} are the distance and pair interaction between two different atoms i and j. This potential function has been widely used [32−34] and shown to be suitable for the simulation of the Ti−Al alloy system.

The initial simulation box size is 50 nm × 50 nm × 50 nm with 8×10^6 atoms in total, as shown in Fig. 1(a). The red and blue atoms correspond to Ti (6×10^6) and Al (2×10^6) atoms, respectively. According to the relationship between average atomic energy and temperature, the solidification temperature of Ti_3Al alloy ranges from 1010 to 965 K. Therefore, a temperature range of 800−1300 K was chosen for the directional solidification simulation. As seen from Fig. 1(b), the initial configuration is divided into three regions along the principal axis X [100]. The leftmost and rightmost 8 nm regions are low-temperature constant (800 K) and high-temperature constant (1300 K) regions, respectively. The temperature in the middle region of 34 nm-thick is not set, but the Berendsen thermostat is adopted in all three regions and the temperature gradient in the middle region forms spontaneously. With the progress of the simulation, the system solidifies from the low-temperature to the high-temperature region. The periodic boundary conditions were applied in principal Y and Z axes. To analyze the structures obtained by the directional solidification, different methods such as common neighbor analysis (CNA) [35] and polyhedral template matching [36] (PTM) were used to determine the grain orientations and various types of atoms with OVITO software.

In order to meticulously investigate the influence of the GNG model on the mechanical properties, the stretching process of Ti_3Al alloy was also simulated by the LAMMPS code. The simulation conditions were: the strain rate was 10^9 s^{-1}, and the loading direction was vertical to the growth direction, which is along the Z axis. Recent studies have found that the grain size has a significant effect on the mechanical properties [37−39]. Therefore, the other two models, namely, the nanograined (NG) and coarse-grained (CG) models, were also used to compare the mechanical properties. To ensure the reliability of the data, the NG and CG models were extracted from the simulated directional solidification structure. Along the growth direction, grains grow and their sizes increase gradually. Therefore, the leftmost and rightmost 10 nm regions of the final directional solidification structure were considered as the NG and CG models, respectively. The stretching process and subsequent visualization of the two models were also analyzed.

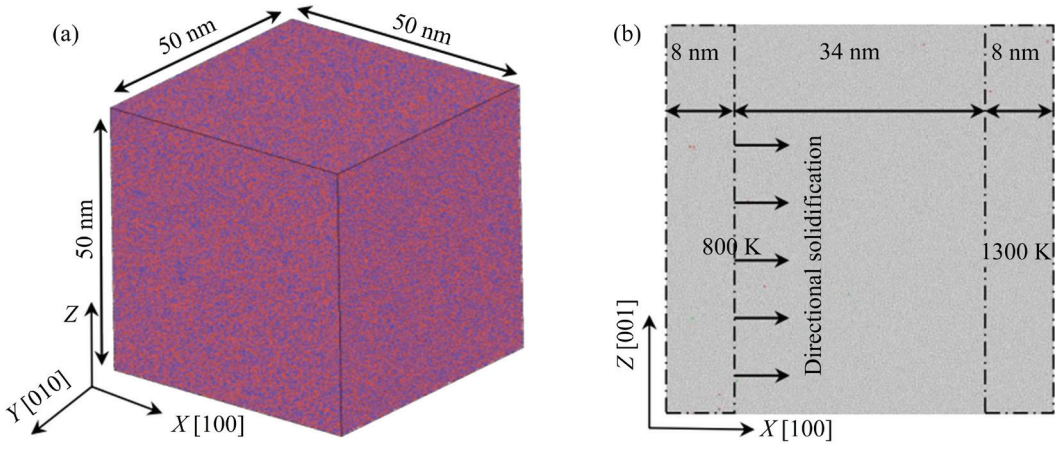

Fig. 1 Schematic of simulation model: (a) Initial simulation box in liquid state; (b) Directional solidification model

3 Results and discussion

3.1 Structural evolution

The structural evolution in the directional solidification process was analyzed by CNA first. It can be seen from Fig. 2(a) that many twins exist in the system, which is consistent with experimental results that a large number of twins form in the directional solidification of Ti_3Al alloy [40,41]. At the initial stage, equiaxed grains are formed first from the liquid alloy, as seen in Figs. 2(a_1) and (a_2). As the solidification front progresses, the initially formed equiaxed grains eventually transform into the columnar grains, as shown in Figs. 2(a_3) and (a_4). To study the grain orientations in directional solidification, the FCC and HCP structures were also analyzed by the PTM method [36], as shown in Fig. 2(b). It is worth noting that some crystal regions are mixed with FCC and HCP structures, which are difficult to obtain the orientation. Therefore, those crystal regions with sole FCC and HCP structures and clear orientations are further shown in Figs. 2(c) and (d), respectively. Comparing Figs. 2(c) and (d), it is observed that the angle between the crystallographic orientation and growth direction of the FCC structure is larger than that of the HCP structure. Besides, the columnar grains occupy a relatively large proportion in the final structure, and the grain size of the columnar grains gradually increases from the formation position to the right end.

To better analyze the directional solidification process, the temperature distribution and the crystallization ratio during the solidification process are presented in Fig. 3. Except for the constant temperature regions on both sides of the box, the temperature almost increases linearly with the distance from the left to the right, as shown in Fig. 3(a), which is consistent with the results obtained

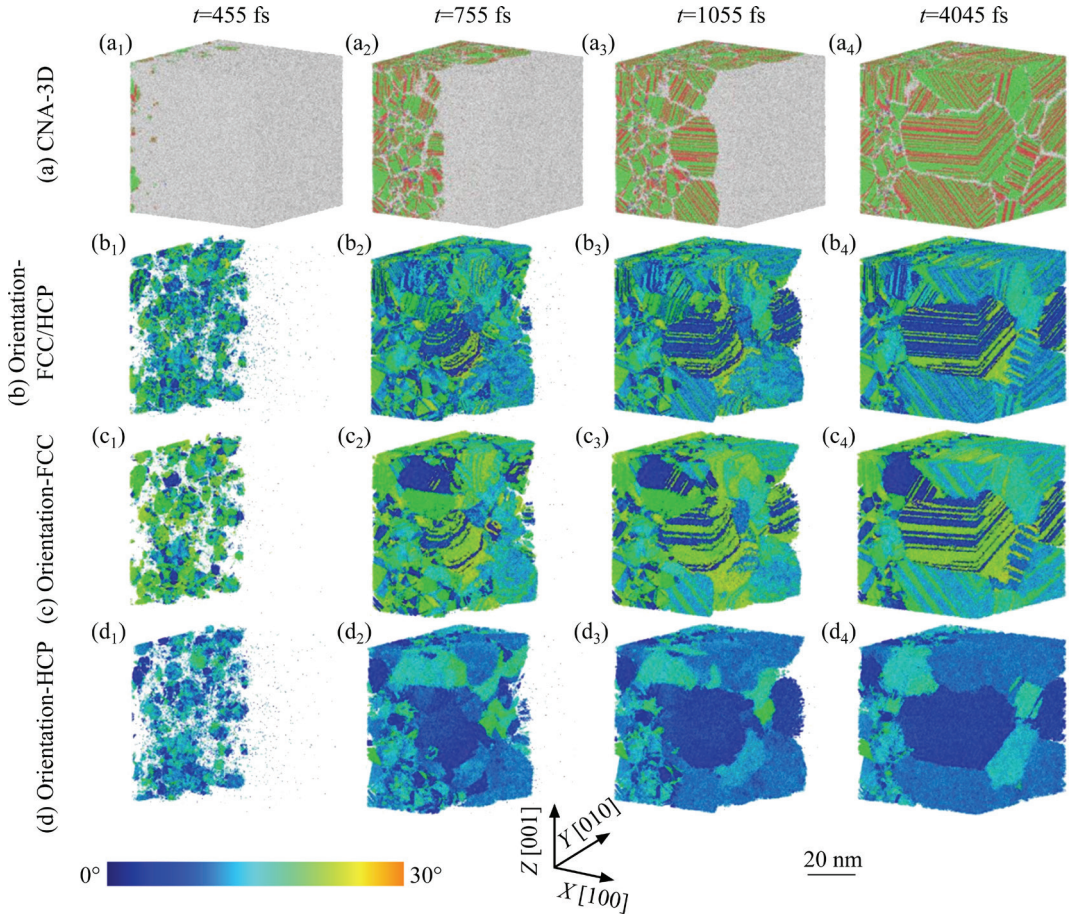

Fig. 2 Visualization of directional solidification process by different methods: (a) CNA analysis; (b) PTM analysis, including both FCC and HCP structures, colored by crystal orientation; (c) PTM analysis, including FCC only, colored by crystal orientation; (d) PTM analysis, containing only HCP, colored according to crystal orientation (The green, red and white colors correspond to FCC, HCP and disordered atoms, respectively, the same below; The color bar represents the deviation degree with the solidification direction)

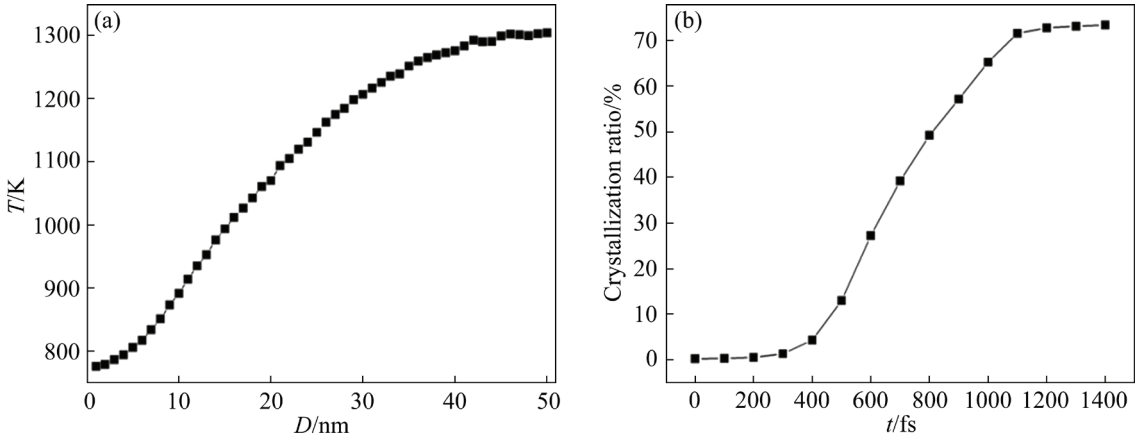

Fig. 3 Several characteristics of simulated directional solidification: (a) Temperature distribution along growth direction *X* [100]; (b) Relationship between crystallization ratio and solidification time

by MAHATA and ASLE ZAEEM [19,20] that the directional solidification proceeds from the low-temperature to the high-temperature region. Moreover, the proportion of crystalline atoms (FCC+HCP) changing with the solidified time was counted for the simulated Ti−Al alloys, and the results are shown in Fig. 3(b). It can be seen that at the initial stage of solidification, there exists an incubation period with a low crystalline ratio. As the solidification front moves, the crystalline ratio increases with solidification time. In particular, the ratio increases to 73% when the solidification time reaches 1100 fs, and then remains almost constant. The rest non-crystal atoms are mainly located at the grain boundaries, as seen in Fig. 2.

Competitive growth of grains usually occurs in the directional solidification [42−44]. Thus, the simulated process was traced from 915 fs to the end of solidification. A series of snapshots are shown in Figs. 4(a_1−c_1), and various views of the solidification front in Figs. 4(a_2−c_2). Three grains exist in the snapshot, which are marked with different colors in Figs. 4(a_1−c_2) for better observation. As the directional solidification proceeds, the grain swallowing phenomenon occurs. As a result, the blue grain becomes larger, while the green grain is gradually suppressed by the surrounding blue and red grains. Eventually, the green grain disappears, as seen in Figs. 4(b_2) and (c_2). To explore why the grain swallowing phenomenon happens in the simulated directional solidification, the box is visualized based on CNA analysis. The obtained *X*−*Z* plane is shown in Fig. 4(d_1), in which α is the angle between the crystallographic orientation and growth direction. As shown in Fig. 4(d_1), four grains are marked as G_1 to G_4 respectively, and their α values are measured. It can be observed that α exhibits the relationship of $\alpha_2 > \alpha_1 > \alpha_4 > \alpha_3$. As the solidification front moves, G_1 and G_2 grains are suppressed by G_3 and G_4 grains. As a result, G_1 and G_2 stop growing, as seen in Fig. 4(d_2). This phenomenon indicates that the grain growth direction is closely related to the direction of heat flow in directional solidification. The smaller the α is, the easier the grain grows, which is consistent with the conclusion obtained by WANG et al [42].

As grain size is closely related to mechanical properties, the sizes of columnar grains in different positions were also studied by slicing the model. The CNA analysis of the slices is shown in Fig. 5(a). Along the heat flow direction, five positions were chosen. For better analysis, the density based spatial clustering of applications with noise (DBSCAN) method was used to identify and extract grains. This method can overcome the problem of misidentifying one grain as two grains due to a twin boundary. The five slices and their cross-sections are shown in Figs. 5(b) and (c), respectively. Different colors represent different grains. The grain sizes along the heat flow direction were calculated using the method proposed by SHIBUTA et al [45], and the results are shown in Fig. 5(d). At the early stage of solidification, like the Images I−III in Fig. 5(c), the grains are separated and small. As they evolve into big grains and merge, only several major grains could be seen in the cross-section. The average grain size exhibits a linear

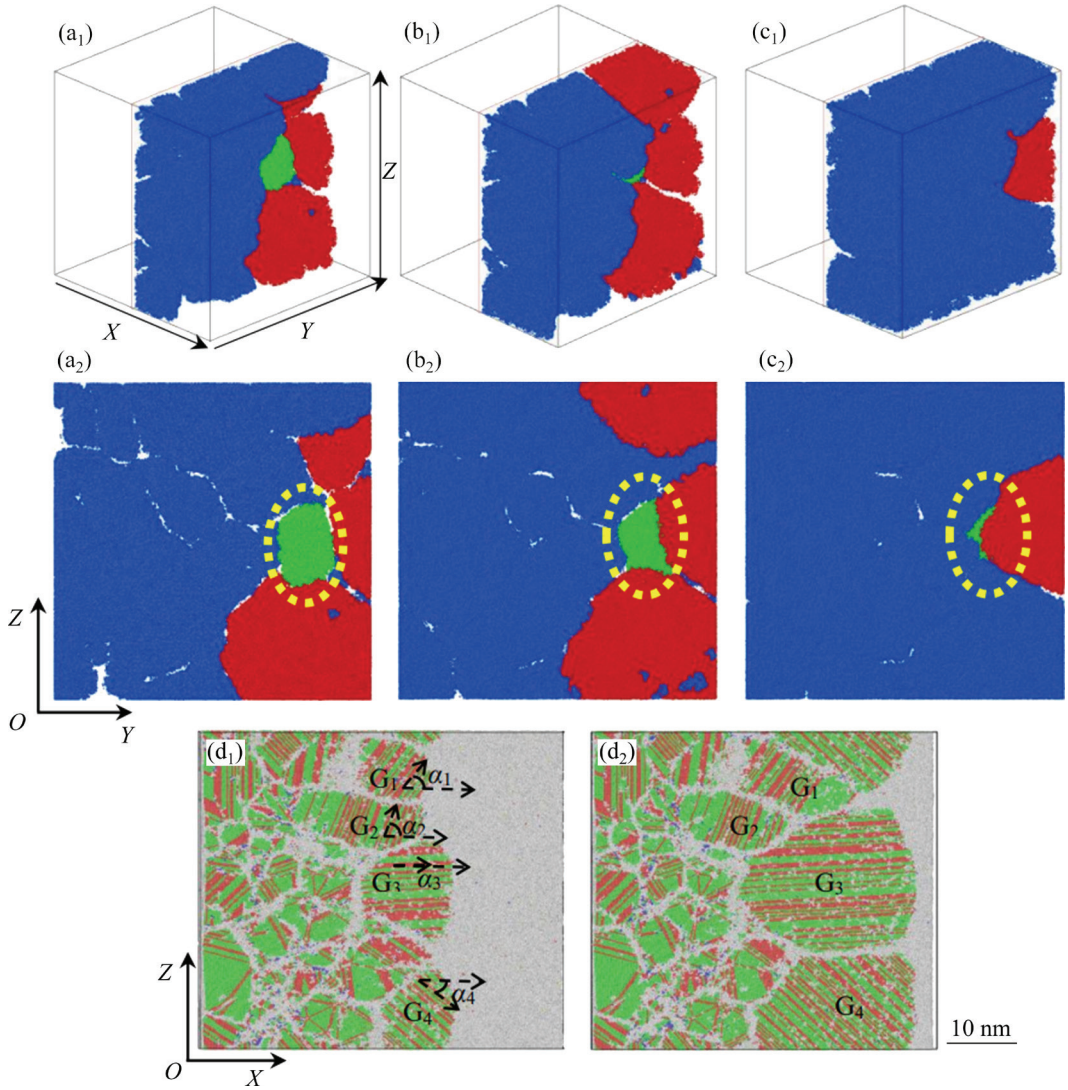

Fig. 4 Competitive growth of grains during directional solidification process at different time: (a_1) t=915 fs; (b_1) t=1055 fs; (c_1) t=1255 fs; (a_2−c_2) Snapshots from view of X axis with time corresponding to (a_1−c_1), respectively; (d_1, d_2) Competitive growth of grains

relationship with the X-axis position. The grain size increases from 8.57 nm at X=5 nm to 16.43 nm at X=45 nm, which is consistent with the grain size relationship obtained from MAHATA and ASLE ZAEEM [19]. The grains will compete with each other, and finally the grains with growth direction close to the heat flow direction will continue to grow up.

3.2 Mechanical properties

Based on the structure characteristics in the simulated directional solidification, the tensile mechanical properties of three models (NG, CG and GNG models) were further investigated. Because the leftmost and rightmost regions are both constant temperature regions, as can be seen in Fig. 6(a), the widths the two regions are almost the same. Combined the variation of grain size from small to large along the X-axis, the leftmost and rightmost regions can be regarded as the NG and CG models, respectively. When the tensile properties of the two models were simulated, atoms were extracted from the 50 nm × 50 nm × 50 nm box first. Then, the uniaxial tension along the [001] direction was applied to the models. Figure 6(b) shows the simulated stress−strain curves of the three models. It can be seen that elastic deformation exists when the strain is within 4% for all three models. The tensile strength of the NG model is around 1.20 GPa after the yield point. As for the CG model, its ultimate tensile strength could reach 1.70 GPa, but the strength decreases after the yield point, and

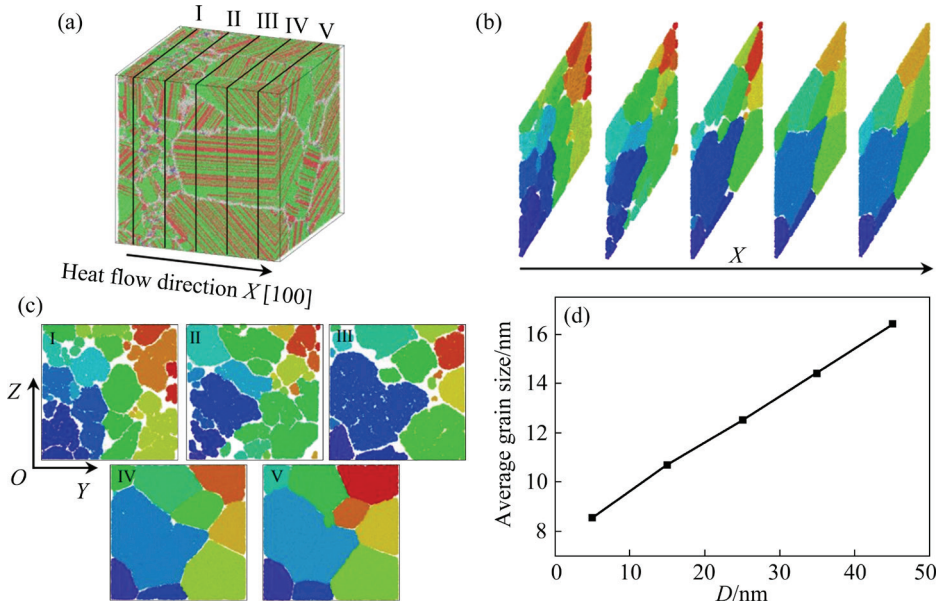

Fig. 5 Evolution of grain size during directional solidification process: (a) Overall simulation box after directional solidification through CNA analysis and illustration of snapshot position; (b) Five snapshots along heat flow direction *X* [100]; (c) Snapshots viewed from *Y*−*Z* plane; (d) Relationship between average grain size obtained from corresponding snapshot and distance

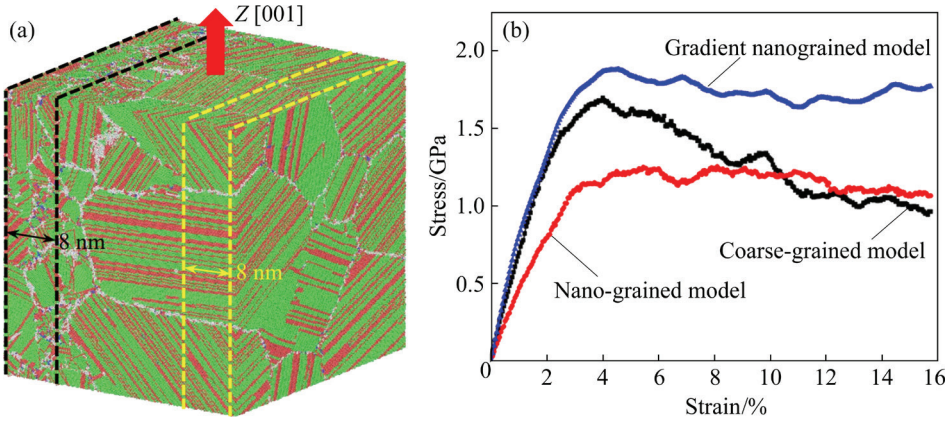

Fig. 6 Mechanical properties for different models: (a) Illustration of three models, leftmost (black area) and rightmost (red area) sides showing NG model and CG model, respectively, whole box showing GNG model; (b) Tensile stress−strain curves for three models along principal axis *Z* [001]

its strength is even lower than that of the NG model after the strain reaches 10%. Compared with the NG and CG models, the tensile strength of the GNG model has better performance. Its ultimate value increases to 1.88 GPa, which is 56.7% and 10.6% higher than the strengths of the NG and CG models, respectively. With the strain increasing from 4% to 10%, the tensile strength of the GNG model decreases slightly and then gradually enhances with high strain. It can also be found that the plasticity of the GNG model is also good, which indicates that the Ti_3Al alloy with GNG structure could possess good strength and ductility at the same time.

To understand why the tensile behaviors of the three models exhibit different features and the deformation mechanism, detailed CNA and shear strain analyses were performed, and the microstructure and shear strain distributions at four strains (ε=0, 5%, 10%, 15%) for the NG model are presented in Figs. 7(a, b). For comparison, the similar analysis results on the GNG model in the same leftmost region are shown in Figs. 7(c, d). Because BCC atoms are rare in system, they are not visible in Fig. 7. The variations of different types of atoms for the NG and GNG models during the stretching process are plotted in Fig. 8. The grain growth phenomenon can be observed in the NG

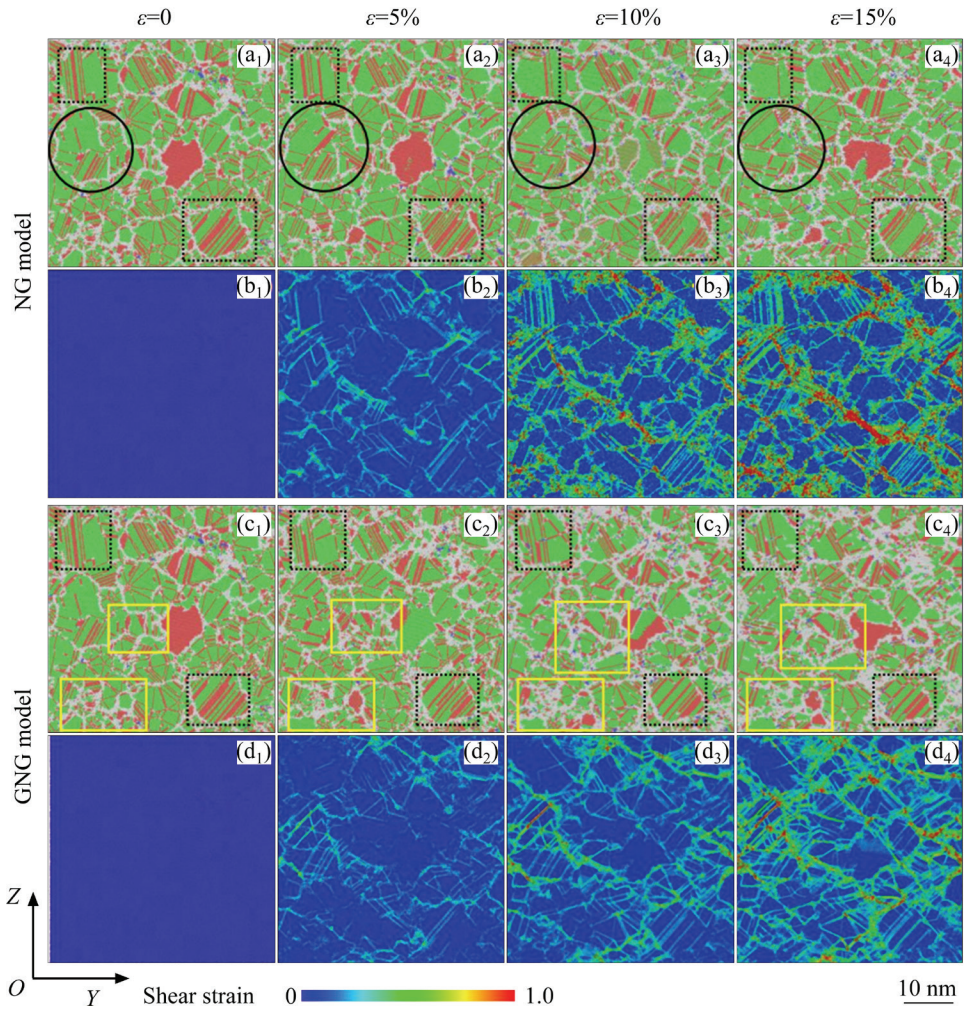

Fig. 7 Microstructure and shear strain distributions in *Y*–*Z* planes of NG and GNG models under various strains (Visualized places for NG and GNG models are the same. The color bar corresponds to the concentration degree of shear strain)

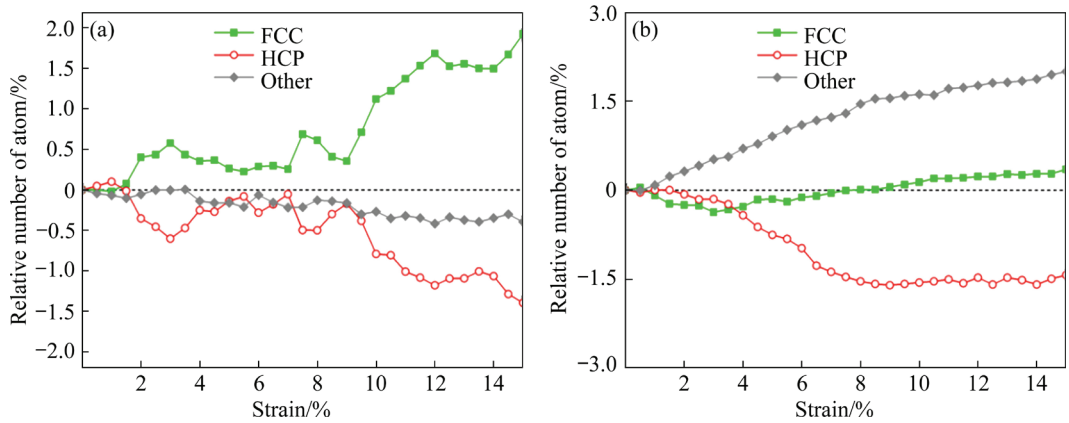

Fig. 8 Relationships between different types of atoms and strains for various models compared to condition of ε=0: (a) NG model; (b) GNG model (The atoms are derived from *Y*–*Z* planes illustrated in Fig. 7 in same place for different strains)

model under tensile loading, which is marked by the black circles in Figs. 7(a_1–a_4), and it can be seen that some grain boundaries disappear with the rise of tensile loading. The detwinning phenomenon occurs consistently with the enhancement of tensile loading, which is marked by the black dashed rectangles in Figs. 7(a_1–a_4). The two phenomena (grain growth and detwinning) in NG model result

in the rise of FCC atoms, the reduction of HCP and other types of atoms in Fig. 8(a). MAHATA and ASLE ZAEEM [19] thought that the driven force of the detwinning is the variation of the excess energy. In this study, no detwinning process occurs in the GNG model at low strain, as indicated by the black dashed rectangles in Figs. 7(c_1, c_2). However, when the strain continues to increase, the detwinning phenomenon can be observed from the black dashed rectangles in Figs. 7(c_2−c_4), resulting in the increase of FCC atoms at a later stage in Fig. 8(b). Besides, in contrast to the NG model, the grain growth phenomenon is not observed in the GNG model, suggesting that the GNG structure could suppress grain growth. On the other hand, the amount of other types of atoms keeps growing with the increasing strain, as shown in the yellow regions in Figs. 7(c_1−c_4). It suggests that more dislocations are generated and they prone to gather at grain boundaries in the GNG model. Comparing the shear strain distribution in Figs. 7(b_1−b_4) and (d_1−d_4), the shear stress in the NG model is concentrated at the local grain boundaries at the strain of 10%, while the shear stress in the GNG model seems to be much more homogeneous and lower than that in NG model even when the strain reaching 15%. It demonstrates that the GNG structure could suppress the grain growth and the shear localization compared to the NG structure under tensile loading, which could contribute to its good strength and plasticity.

In addition, the visualization and shear strain distribution analyses of the CG and GNG models were also compared. The four strains of the shear strain snapshots were still 0, 5%, 10% and 15%, and the results are shown in Fig. 9. The atom-type transitions of the two models during the stretching process are compared to the undeformed condition in Fig. 10. As the strain increases from 0 to 5%, the detwinning process plays a dominant role for the

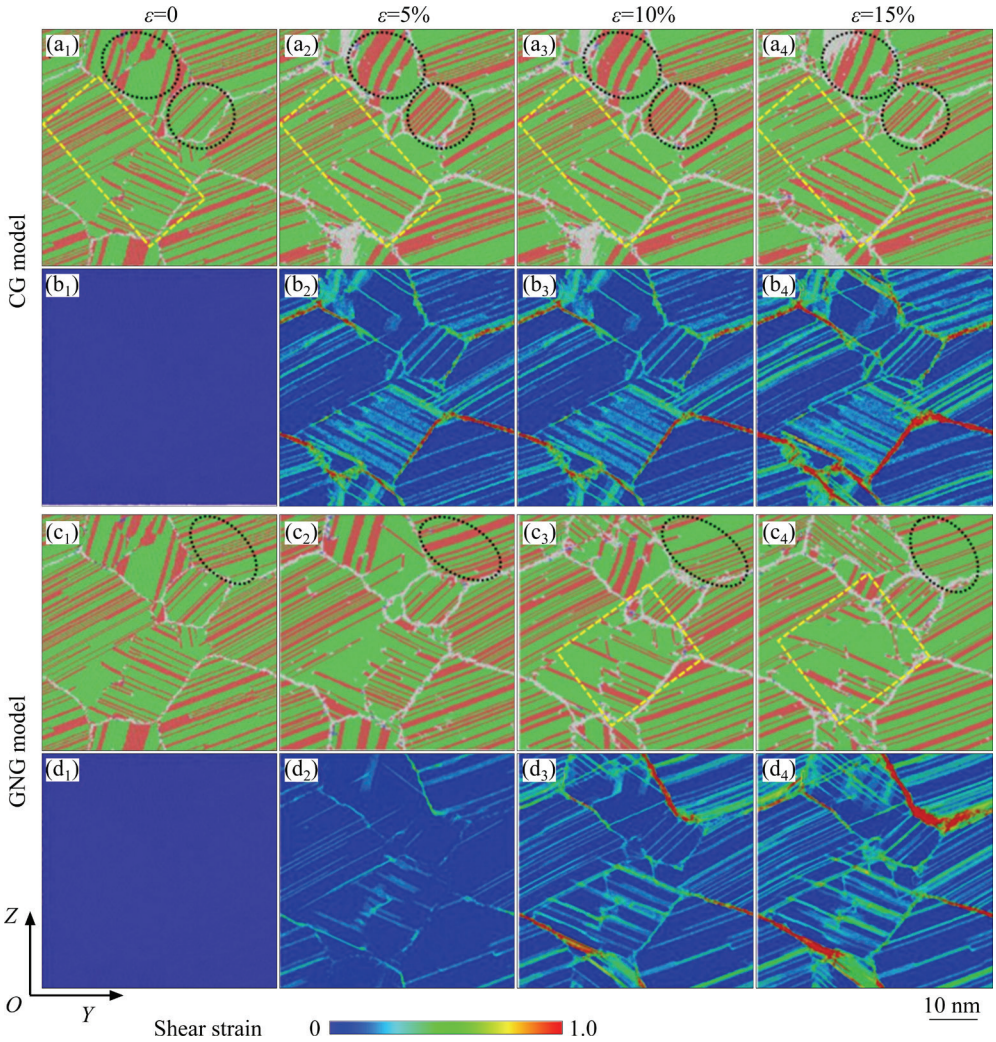

Fig. 9 CNA analyses and shear strain distributions in *Y*−*Z* planes of CG and GNG models under various strains (The visualized places for the two models are the same. The color bar corresponds to the concentration degree of shear strain)

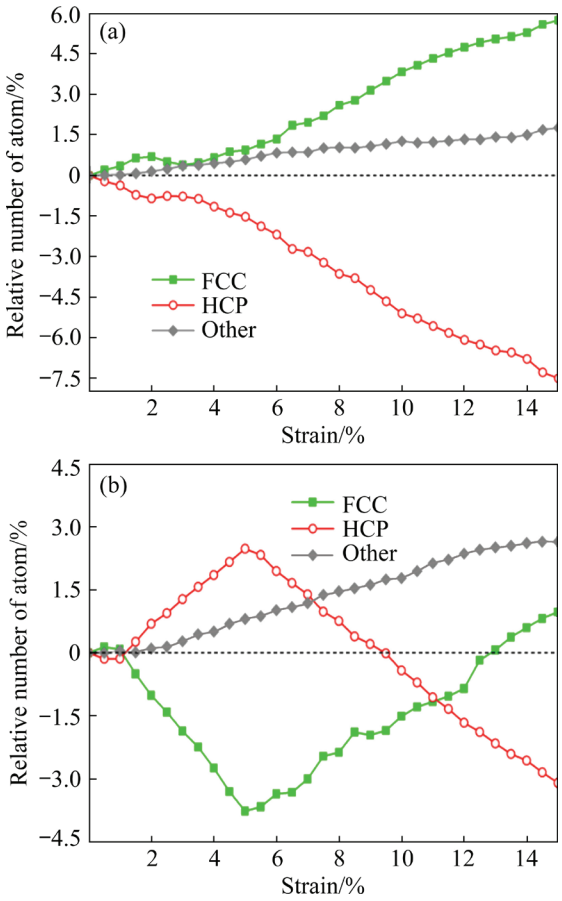

Fig. 10 Relationships between different types of atoms and strains for various models compared to condition of ε=0: (a) CG model; (b) GNG model (The atoms are derived from the *Y*−*Z* planes illustrated in Fig. 9 in same place for different strains)

CG model, as can be seen from the yellow regions in Figs. 9(a_1, a_2). However, there are more dislocations and stacking faults (red color) generated at the same time, which could be seen from the black dash ellipses in Figs. 9(a_1, a_2). The combined effects lead to a slight decrease of HCP atom and a minor rise of FCC and other types of atoms, as seen in Fig. 10(a). In the GNG model, dislocation nucleation is a more effective factor in the strain range from 0 to 5%, which leads to the rapid growth of the HCP atoms, as can be seen in Fig. 10(b). When the strain increases to a high value, the detwinning process plays a critical role in both CG and GNG models, as indicated by the marked black dash ellipses in Figs. 9(a_2−a_4) and (c_2−c_4). So, the number of FCC atom increases rapidly in both Figs. 10(a) and (b) as the strain exceeds 5%, accompanied by a sharp reduction of HCP atoms. But comparing the two models, the detwinning phenomenon is more obvious in CG model. Besides, the amount of other type atoms still slightly rises for the two models due to more dislocations during the deformation process. It is worth noting that the cross stacking faults and dislocations (marked in the figures) could convert the uniaxial stress to multi-axial stresses [13,46]. As indicated by the yellow regions in Figs. 9(c_3, c_4), the interactions of stacking exist in the GNG model. The special gradient faults and dislocations can provide extra strain hardening to enhance the strength and ductility of the GNG model, which was reported by CHENG et al [11,47]. Furthermore, it could be found that the shear strain is concentrated at some grain boundaries in the CG model at the strain of 5%, as shown in Fig. 9(b_2), and the strain localization phenomenon is more obvious with increasing strain. The similar phenomenon is observed in the GNG model until the strain reaches 10%, as seen in Fig. 9(d_3), which indicates that the mechanical properties could be improved if the alloy has a GNG structure. The lower strain localization is also a vital factor to enhance the mechanical performance [11,47−49]. In summary, compared to the NG and CG structures, the GNG structure could restrict the strain localization and promote more cross dislocations during the stretching process, which could contribute to the good strength and plasticity.

4 Conclusions

(1) In the early stage of the directional solidification, the alloy is solidified in the form of equiaxed crystals. As the directional solidification front progresses, the microstructure will transform into columnar crystals, and the columnar grains will gradually elongate. The average grain size of the directional solidified Ti_3Al alloy follows a linear pattern from the low-temperature region to the high-temperature region. The morphology of directional solidification structure obtained by MD simulation is consistent with experiment results.

(2) During the directional solidification process, competitive growth is found among grains. The closer the grain growth direction is to the heat flow direction, the easier the grain growth is.

(3) The tensile loading simulation indicates that the GNG structure formed by directional solidification has better mechanical performance

than the uniform CG and NG structures. The GNG structure suppresses strain localization and grain growth in small grain regions and promotes cross dislocations in large grain regions, leading to a higher tensile strength and ductility.

CRediT authorship contribution statement

Peng-fei ZOU: Writing − Original draft, Simulation; **Chang LI:** Building the model of the simulation; **Zhao-yang HOU:** Writing − Review & editing, Conceptualization, Funding acquisition; **Jia-yi SUN:** Data curation; **Quan-hua GAO:** Data curation; **Ke-fan LI:** Methodology; **Zhen WANG:** Methodology; **Ke-jun DONG:** Writing − Review & editing.

Declaration of competing interest

The authors declare that they have no known competing financial interests or personal relationships that could have appeared to influence the work reported in this paper.

Acknowledgments

The authors would like to acknowledge the support provided by the National Natural Science Foundation of China (No. 52201103), and the Natural Science Basis Research Plan in Shaanxi Province of China (No. 2023JCYB445). This work is also supported by the Fundamental Research Funds for the Central Universities of CHD (Nos. 300102122201, 300102122106).

References

[1] MAYER S, ERDELY P, FISCHER F D, HOLEC D, KASTENHUBER M, KLEIN T, CLEMENS H. Intermetallic β-solidifying γ-TiAl based alloys — From fundamental research to application [J]. Advanced Engineering Materials, 2017, 19: 1600735.

[2] CHEN Guang, PENG Ying-bo, ZHENG Gong, QI Zhi-xiang, WANG Min-zhi, YU Hui-chen, DONG Cheng-li, LIU C T. Polysynthetic twinned TiAl single crystals for high-temperature applications [J]. Nature Materials, 2016, 15: 876−881.

[3] ZHANG Jian-yu, WANG Yan-hui, ZHENG LÜ, CHEN Qing-an, CHEN Ya-yu, LI He-zong. Formation mechanism and growth kinetics of $TiAl_3$ phase in cold-rolled Ti/Al laminated composites during annealing [J]. Transactions of Nonferrous Metals Society of China, 2022, 32: 524−539.

[4] YUE Xiao-an, SHEN Jun, XIONG Yi-long, LI Qiu-dong, ZHENG Shao-kai. Microstructure, fracture toughness and high-temperature tensile property of large size Ti−46Al−5Nb−0.18C−0.3Si alloy with oriented lamella by electromagnetic confinement directional solidification [J]. Materials Science and Engineering A, 2021, 812: 141139.

[5] LIU Yang-li, XUE Xiang, TAN Ying-mei, FANG Hong-ze, CUI Hong-zhi, CHEN Rui-run. Microstructure formation and elevated temperature mechanical properties of directionally solidified Ti44Al6Nb1Cr alloy [J]. Materials Science and Engineering A, 2020, 797: 140038.

[6] LIU Yang-li, XUE Xiang, FANG Hong-ze, TAN Ying-mei, CHEN Rui-run, SU Yan-qing, GUO Jing-jie. The growth behavior of columnar grains in a TiAl alloy during directional induction heat treatments [J]. CrystEngComm, 2020, 22: 1188−1196.

[7] WANG Qiang, ZENG Liang-cai, DING Hong-sheng, CHEN Rui-run, GUO Jing-jie, FU Heng-zhi. On the high temperature deformation of a directionally solidified γ-TiAl alloy [J]. Materials Science and Engineering A, 2019, 758: 19−27.

[8] GAO Yu-bi, LI Xiu-yan, MA Yuan-jun, KITCHEN M, DING Yu-tian, LUO Quan-shun. Formation mechanism and wear behavior of gradient nanostructured Inconel 625 alloy [J]. Transactions of Nonferrous Metals Society of China, 2022, 32: 1910−1925.

[9] LI Xi, FAUTRELLE Y, REN Zhong-ming. Influence of an axial high magnetic field on the liquid−solid transformation in Al−Cu hypoeutectic alloys and on the micro structure of the solid [J]. Acta Materialia, 2007, 55: 1377−1386.

[10] FANG T, LI W, TAO N, LU K. Revealing extraordinary intrinsic tensile plasticity in gradient nano-grained copper [J]. Science, 2011, 331: 1587−1590.

[11] CHENG Zhao, ZHOU Hao-fei, LU Qiu-hong, GAO Hua-jian, LU Lei. Extra strengthening and work hardening in gradient nanotwinned metals [J]. Science, 2018, 362: eaau1925.

[12] WU Xiao-lei, ZHU Yun-tian. Heterogeneous materials: A new class of materials with unprecedented mechanical properties [J]. Materials Research Letters, 2017, 5: 527−532.

[13] WU Xiao-lei, JIANG Ping, CHEN Liu, YUAN Fu-ping, ZHU Yuntian. Extraordinary strain hardening by gradient structure [J]. Proceedings of the National Academy of Sciences of the United States of America, 2014, 111: 7197−7201.

[14] TIAN Xiao-lin, ZHAO Yu-hong, PENG Dun-wei, GUO Qing-wei, GUO Zhen, HOU Hua. Phase-field crystal simulation of evolution of liquid pools in grain boundary pre-melting regions [J]. Transactions of Nonferrous Metals Society of China, 2021, 31: 1175−1188.

[15] KARMA A. Phase-field formulation for quantitative modeling of alloy solidification [J]. Physical Review Letters, 2001, 87: 115701.

[16] GUO Chun-wen, WENG Kang-rong, WANG Jjin-cheng, ZHAO Hong-linag, DONG Xianglei, FAN Yu-heng, LI Jun-jie. Competitive growth of diverging columnar grains during directional solidification: A three-dimensional phase-field study [J]. Computational Materials Science, 2022, 210: 111061.

[17] XING Hui, JI Ming-yue, DONG Xiang-lei, WANG Yu-ming, ZHANG Li-min, LI Shuang-ming. Growth competition between columnar dendrite and degenerate seaweed during directional solidification of alloys: Insights from multi-phase field simulations [J]. Materials & Design, 2020, 185: 108250.

[18] DAS A, JI S, FAN Z. Morphological development of solidification structures under forced fluid flow: A Monte-Carlo simulation [J]. Acta Materialia, 2002, 50: 4571−4585.

[19] MAHATA A, ASLE ZAEEM M. Effects of solidification defects on nanoscale mechanical properties of rapid directionally solidified Al−Cu Alloy: A large scale molecular dynamics study [J]. Journal of Crystal Growth, 2019, 527: 125255.

[20] MAHATA A, ASLE ZAEEM M. Insights on solidification of Mg and Mg−Al alloys by large scale atomistic simulations [C]//Magnesium Technology. Cham: Springer, 2020: 51−53.

[21] BAHRAMYAN M, MOUSAVIAN R T, CARTON J G, BRABAZON D. Nano-scale simulation of directional solidification in TWIP stainless steels: A focus on plastic deformation mechanisms [J]. Materials Science and Engineering A, 2021, 812: 140999.

[22] HU Lin, TIAN Zean, LIANG Yong-chao, GAO Ting-hong, CHEN Qian, ZHENG Quan, LUO Yu-xi, XIE Quan. The role of TCP structures in glass formation of $Ni_{50}Ag_{50}$ alloys [J]. Journal of Alloys and Compounds, 2022, 897: 162743.

[23] KAREWAR S, SIETSMA J, SANTOFIMIA M J. Effect of pre-existing defects in the parent fcc phase on atomistic mechanisms during the martensitic transformation in pure Fe: A molecular dynamics study [J]. Acta Materialia, 2018, 142: 71−81.

[24] XU Hao-dong D, BAO Hong-wei, LI Yan, BAI Hui-zhong, MA Fei. Atomic scale insights into the rapid crystallization and precipitation behaviors in FeCu binary alloys [J]. Journal of Alloys and Compounds, 2021, 882: 160725.

[25] GUO Jing-jie, LI Xin-zhong, SU Yan-qing, WU Shi-ping, LI Bang-sheng, FU Heng-zhi. Phase-field simulation of structure evolution at high growth velocities during directional solidification of $Ti_{55}Al_{45}$ alloy [J]. Intermetallics, 2005, 13: 275−279.

[26] SINGER H M, SINGER I, JACOT A. Phase-field simulations of α−γ precipitations and transition to massive transformation in the Ti−Al alloy [J]. Acta Materialia, 2009, 57: 116−124.

[27] HAO Meng-yuan, LI Pei, LI Xue-xiong, ZHANG Tian-long, WANG Dong, SUN Qiao-yan, LIU Li-bin, LI Jin-shan, CUI Yu-you, YANG Rui, XU Dong-sheng. Heterogeneous precipitate microstructure in titanium alloys for simultaneous improvement of strength and ductility [J]. Journal of Materials Science & Technology, 2022, 124: 150−163.

[28] LI Jun-jie, WANG Zhi-jun, WANG Ya-qin, WANG Jin-cheng. Phase-field study of competitive dendritic growth of converging grains during directional solidification [J]. Acta Materialia, 2012, 60: 1478−1493.

[29] VIARDIN A, ZOLLINGER J, STURZ L, APEL M, EIKEN J, BERGER R, HECHT U. Columnar dendritic solidification of TiAl under diffusive and hypergravity conditions investigated by phase-field simulations [J]. Computational Materials Science, 2020, 172: 109358.

[30] PLIMPTON S. Fast parallel algorithms for short-range molecular dynamics [J]. Journal of Computational Physics, 1995, 117: 1−19.

[31] ZOPE R R, MISHIN Y. Interatomic potentials for atomistic simulations of the Ti−Al system [J]. Physical Review B, 2003, 68: 024102.

[32] GAO Yue, GAO Ting-hong, LI Lian-xin, XIE Yuan, CHEN Qian, TIAN Zean, LIANG Yong-chao, WANG Bei. Evolution of dislocation and twin structures in Ti_3Al during solidification [J]. Vacuum, 2021, 194: 110525.

[33] FENG Rui-cheng, WANG Mao-mao, LI Hai-yan, QI Yong-nian, WANG Qi, RUI Zhi-yuan. Micromechanism of cold deformation of two-phase polycrystalline Ti−Al alloy with void [J]. Materials, 2019, 12(1): E184.

[34] ZHANG Jin-hu, TENG Chun-yu, MENG Zhi-chao, XU Hai-sheng, YANG Liang, XU Dong-sheng, YANG Rui. Selection and mechanical evaluation of γ/γ boundary in γ-TiAl alloy[J]. Intermetallics, 2020, 126: 106946.

[35] HONEYCUTT J D, ANDERSEN H C. Molecular dynamics study of melting and freezing of small Lennard−Jones clusters [J]. The Journal of Physical Chemistry, 1987, 91: 4950−4963.

[36] LARSEN P M, SCHMIDT S, SCHIØTZ J. Robust structural identification via polyhedral template matching [J]. Modelling and Simulation In Materials Science And Engineering, 2016, 24: 055007.

[37] WANG Bo, CHEN Xian-hua, PAN Fu-sheng, MAO Jian-jun, FANG Yong. Effects of cold rolling and heat treatment on microstructure and mechanical properties of AA 5052 aluminum alloy [J]. Transactions of Nonferrous Metals Society of China, 2015, 25: 2481−2489.

[38] XIAO Hong-yu, LI Yu-gang, GENG Ji-wei, LI Hong-ping, WANG Ming-liang, CHEN Dong, LI Zhu-guo, WANG Hao-wei. Effects of nano-sized TiB_2 particles and Al_3Zr dispersoids on microstructure and mechanical properties of Al−Zn−Mg−Cu based materials [J]. Transactions of Nonferrous Metals Society of China, 2021, 31: 2189−2207.

[39] XU Wen-wu, DÁVILA L P. Tensile nanomechanics and the Hall−Petch effect in nanocrystalline aluminium [J]. Materials Science and Engineering A, 2018, 710: 413−418.

[40] CUI Ning, WU Qian-qian, WANG Jin, LV Bin-jiang, KONG Fan-tao. The directional solidification, microstructural characterization and deformation behavior of β-Solidifying TiAl alloy [J]. Materials, 2019, 12(8): 1203.

[41] DING X F, LIN J P, ZHANG L Q, SU Y Q, CHEN G L. Microstructural control of TiAl−Nb alloys by directional solidification [J]. Acta Materialia, 2012, 60: 498−506.

[42] WANG Jin-cheng, GUO Chun-wen, LI Jun-jie, WANG Zhi-jun. Recent progresses in competitive grain growth during directional solidification [J]. Acta Metallurgica Sinica, 2018, 54: 657−668.

[43] YANG Chu-bin, LIU Lin, ZHAO Xin-bao, WANG Ning, ZHANG Jun, FU Heng-zhi. Competitive grain growth mechanism in three dimensions during directional solidification of a nickel-based superalloy [J]. Journal of Alloys and Compounds, 2013, 578: 577−584.

[44] WANG Hai-wei, ZHANG Xiao-li, MENG Jie, YANG Jin-xia, YANG Yan-hong, ZHOU Yi-zhou, SUN Xiao-feng. A new model of competitive grain growth dominated by the solute field of the nickel-based superalloys during directional solidification [J]. Journal of Alloys and Compounds, 2021, 873: 159794.

[45] SHIBUTA Y, OGUCHI K, TAKAKI T, OHNO M. Homogeneous nucleation and microstructure evolution in

million-atom molecular dynamics simulation [J]. Scientific Reports, 2015, 5: 13534.
[46] LI Wen-bin, YUAN Fu-ping, WU Xiao-lei. Atomistic tensile deformation mechanisms of Fe with gradient nano-grained structure [J]. AIP Advances, 2015, 5: 087120.
[47] CHENG Zhao, BU Lin-feng, ZHANG Yin, WU Heng-an, ZHU Ting, GAO Hua-jian, LU Lei. Unraveling the origin of extra strengthening in gradient nanotwinned metals [J]. Proceedings of the National Academy of Sciences of the United States of America, 2022, 119: e2116808119.
[48] WANG J J, TAO N R, LU K. Revealing the deformation mechanisms of nanograins in gradient nanostructured Cu and CuAl alloys under tension [J]. Acta Materialia, 2019, 180: 231−242.
[49] LONG Jian-zhou, PAN Qing-song, TAO Nai-rong, DAO Ming, SURESH S, LU Lei. Improved fatigue resistance of gradient nanograined Cu [J]. Acta Materialia, 2019, 166: 56−66.

定向凝固条件下 Ti_3Al 合金中梯度纳米结构的形成机制与力学行为——原子尺度研究

邹鹏飞[1]，李 昌[1]，侯兆阳[1]，Jia-yi SUN[2]，高全华[1]，李克凡[1]，王 真[1]，Ke-jun DONG[3]

1. 长安大学 理学院，西安 710064；
2. Faculty of Natural, Mathematics & Engineering Sciences, King's College London, London, WC2R 2LS, United Kingdom;
3. School of Engineering, Design and Built Environment, Western Sydney University, Penrith, NSW 2751, Australia

摘 要：通过分子动力学(MD)模拟方法对 Ti_3Al 合金在定向凝固条件下的生长机理进行系统研究，并通过对比纳米晶(NG)、粗晶(CG)和梯度纳米晶(GNG)合金，研究 Ti_3Al 合金的结构力学性能。结果表明，在凝固过程中 Ti_3Al 相优先生长为等轴晶组织，随后逐渐演变为柱状粒，并最终形成梯度纳米晶结构。此时，晶粒在与凝固方向平行的方向优先生长。此外，研究还发现，相较于 NG 和 CG 结构，GNG 结构定向凝固合金具有更高的抗拉强度和更好的延展性。GNG 结构不仅有效抑制了小晶粒区域的应变局域化和晶粒生长，而且促进了较大晶粒区域的位错形成，从而获得更好的力学性能。

关键词：定向凝固；Ti_3Al 合金；分子动力学模拟；梯度纳米结构

(Edited by Xiang-qun LI)